

Some Features of Photocurrent Generation in Single- and Multibarrier Photodiode Structures

A. V. Karimov[^] and D. M. Yodgorova

Physical-Technical Institute, Physics-Sun Scientific Production Association, ul. G. Mavlyanov 2b,
Uzbekistan Academy of Sciences, Tashkent, 100084 Uzbekistan

[^]e-mail: karimov@uzsci.net

Submitted May 14, 2009; accepted for publication September 15, 2009

Abstract—In contrast to single barrier photodiode structures, multibarrier ones exhibit the effect of increasing the number of photogenerated carriers in the entire range of operating voltages, whereas the photocurrent generation in avalanche and injection photodiodes is characterized by the threshold behavior and is associated with changes in the dark carrier density. The suggested interpretation of the effect of internal photoelectric amplification will make it possible to estimate experimental current or voltage gains and detect photoelectric amplification in photodiode structures irrespective of their type.

DOI: 10.1134/S1063782610050179

1. INTRODUCTION

Currently, optical signal transmission begins to replace electrical methods of data transmission. Optical transmission methods feature high noise immunity, high data transmission rate, and the possibility of transmitting several data flows through a single optical cable. Optical signal reception and transmission are performed using a laser or light-emitting diode, information carrier, i.e., optical fiber, and a photodiode-based detector. The rapid development of fiber-optical systems of data transmission is caused by continuing improvement of optical fibers [1] and optical amplifiers [2], which, in turn, requires the development of corresponding emitters [3] and photodetectors [4]. However, the existing principles of photocurrent generation and photodetector types are very different. In addition, new technological designs become to be developed, which facilitate the development of non-conventional photodetectors based on low-dimensional and other effects [5]. To this end, it is reasonable to consider the features of photodiode structures and photocurrent generation and photocurrent amplification mechanisms, their intimate relationship with photosensitivity conditions, and some features of the next-generation photocurrent generation in two- and three-barrier photodetectors.

This study is devoted to the analysis of some physical processes of photocurrent generation in single- and two-base photodiode structures and the development of assessment criteria for the internal photocurrent amplification.

The requirements for photosensitive structures are continuously becoming more stringent. A number of conventional devices, it can be said, have become classical; however, new modifications with distinctive fea-

tures are being developed [6]. To study photocurrent generation, we fabricated special structures, i.e., photodiodes with a graded-gap base region, two-barrier injection-field and three-barrier photodiodes [7, 8]. They are of interest as detectors of weak optical signals for photodetecting units of multipurpose devices, e.g., remote control of technological processes, security systems, telecommunication, and others.

2. EXPERIMENTAL SAMPLES

When choosing the (Au + Zn)–*p*-AlGaAs–*n*-GaAs–(Sn) diode heterostructure with a graded-gap base region, we proceeded from the fact that its photosensitivity can be increased by inducing a pulling internal electric field.

A front photodetecting layer with positive gradient in such a photodiode heterostructure was obtained in a piston cassette providing a linear increase in the Al fraction during growth of an isothermal liquid epitaxy layer. In particular, the heterolayer band gap increases from 1.43 to 1.8 eV from the interface with *n*-GaAs to the surface. The configuration of a heterostructure with graded-gap photodetecting surface is shown in Fig. 1. The carrier density in the *n*-GaAs region 400 μm thick is $2 \times 10^{16} \text{ cm}^{-3}$; in the epitaxial layer *p*-AlGaAs ~1.6 μm thick, it is $4 \times 10^{18} \text{ cm}^{-3}$. Ohmic contacts to the front surface were formed by vacuum deposition through an Au + Zn alloy mask; on the *n*-GaAs backside, a continuous Sn layer was also vacuum-deposited. As a result, (Au + Zn)–*p*-AlGaAs–*n*-GaAs–(Sn) photodiode structures were fabricated. Their current–voltage (*I*–*V*) characteristics (Fig. 2) show that the dark current in such a heterostructure at a voltage of 200 mV is 10^{-9} A . The current under illu-

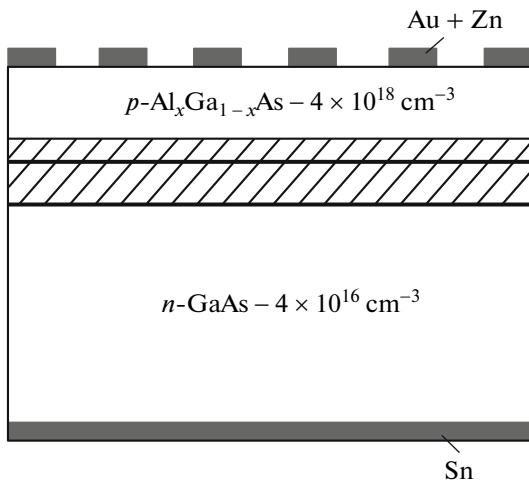


Fig. 1. Configuration of the heterostructure (Au + Zn)–*p*-AlGaAs–*n*-GaAs–(Sn) with graded-gap photodetecting surface. The parameter x in the $\text{Al}_x\text{Ga}_{1-x}\text{As}$ alloy formula was varied from 0 to 0.3.

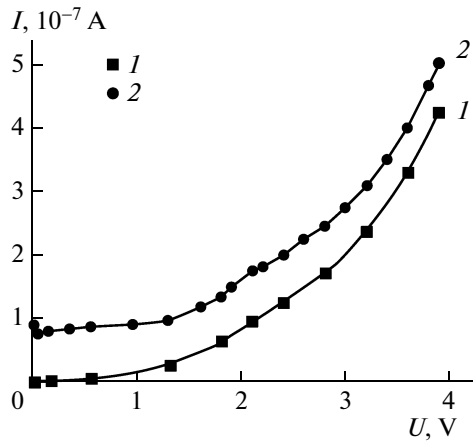


Fig. 2. Current–voltage characteristics of the *p*-AlGaAs–*n*-GaAs structure with graded-gap photodetecting region, measured (1) in the dark and (2) upon exposure to radiation of a lamp with $\lambda = 0.55 \mu\text{m}$.

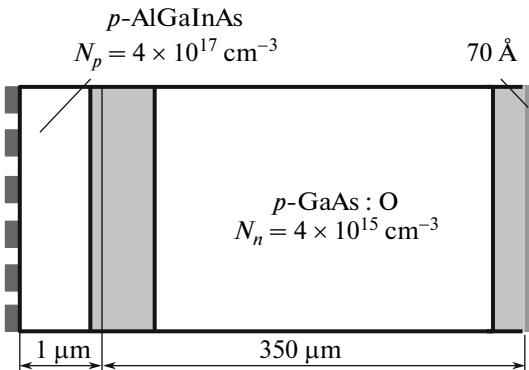


Fig. 3. Configuration of the two-barrier photodiode under study.

mination at zero bias is ten times higher than the dark current ($9 \times 10^{-8} \text{ A}$). Here it should be noted that “light” characteristics were measured upon exposure to radiation of a halogen lamp with a maximum at a wavelength of $0.55 \mu\text{m}$.

Bilaterally sensitive two-barrier *p*–*n*–*m* structures (*m* is a metal) were fabricated with an emitter region thickness ($1 \mu\text{m}$) smaller than the light penetration depth and with a carrier concentration ($4 \times 10^{17} \text{ cm}^{-3}$) a hundred times higher than that ($4 \times 10^{15} \text{ cm}^{-3}$) in the base region. In turn, the base region thickness ($d = 350 \mu\text{m}$) was much larger than the diffusion length of minority carriers ($d \gg L_{p,n}$), which is required for injection diodes. The configuration of the p –($\text{Al}_{0.08}\text{Ga}_{0.82}\right)_{0.9}\text{In}_{0.1}\text{As}$ –*n*-GaAs–Au two-barrier structure under study is shown in Fig. 3, where we can see that it contains two oppositely connected junctions (*p*–*m*, *n*–*m*).

Another feature of this structure is that it becomes an analog of a long diode, i.e., the injection diode. When a positive voltage is applied to the *p*-type layer. As the applied voltage polarity is changed, it can function as a photodetector, approaching properties of *p*–*i*–*n* diodes, but with a voltage-controlled depletion region thickness.

The (Au)–*n*-AlGaAs–*p*-GaAs–(Ag) three-barrier photodiode structure was fabricated on the basis of the *p*–*n* junction in which the *p*-type region is a bulk GaAs crystal with $N_A = (5–7) \times 10^{15} \text{ cm}^{-3}$ and the *n*-type region is an AlGaAs epitaxial layer with $N_D = 2 \times 10^{16} \text{ cm}^{-3}$. The thickness of the *n*-type region grown by liquid epitaxy is $1.5–2 \mu\text{m}$. On the *p*-type region back-side, a rectifying (100 Å) Ag contact was formed; on the *n*-type region surface, a semitransparent Au layer potential barrier was deposited as shown in Fig. 4. The area of the structures was $8–80 \text{ mm}^2$; the specific capacitance was $\sim 0.2 \text{ pF/mm}^2$.

Current–voltage characteristics of both photodiode structures exposed to light from the heterolayer side are shown in Figs. 5a and 5b. The observed differences in the current dependences can be explained by the difference between the processes and regions of carrier photogeneration and the specific dependence of the dark current on voltage. In the two-barrier structure, photocarriers are generated in the heterolayer; in the three-barrier structure, they are generated in the space charge region of potential barriers. In all samples, we observed “dark” and “light” currents.

For all samples, we have dark and light curves, from which we can estimate the experimental photocurrent, i.e., the difference of the light and dark currents

$$I^{\text{photo}} = I^{\text{light}} - I^{\text{dark}}$$

independently of their generation mechanism. A comparison of photoelectric characteristics of the grown photodiode structures shows that the photocurrent in the photodiode structure with graded-gap base region

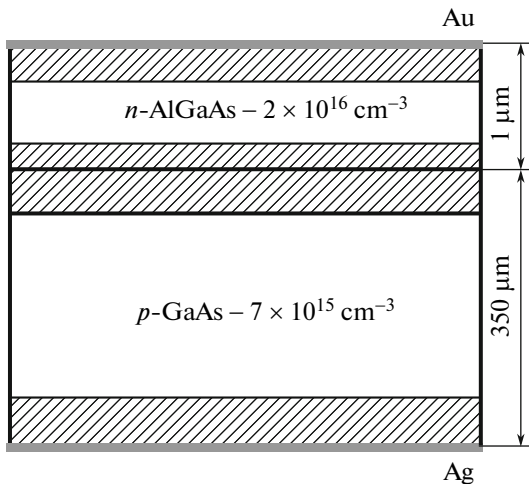


Fig. 4. Configuration of the (Au)-*n*-AlGaAs-*p*-GaAs-(Ag) three-barrier heterostructure under study.

decreases as the operating voltage increases from 0 to 4 V (Fig. 2). As for the injection-field photodiode, we observe an increase in the photocurrent followed by a slowed increase in the dark current (Fig. 5a); in the three-barrier structure, the photocurrent gradually increases with voltage (Fig. 5b). In this case, the dark current of the structure with graded-gap base region monotonically increases beyond 1 V; in the two-barrier *p-n-m* structure, the dark current increases only at voltages above 60 V. In the three-barrier structure, the reverse dark current varies almost linearly with voltage.

At the same time, in the single-barrier hetero-*p-n* structure, we observe a decrease in the photocurrent with voltage; in contrast, in two- and three-barrier structures, we observe its increase [9, 10]. This effect of increasing the photocurrent is associated with the internal photoelectric amplification caused by processes in the space charge region, where the photocarrier generation rate begins to dominate over the concentration increment of carriers generating the reverse dark current as the applied voltage increases. Physically, this phenomenon occurs when carrier injection through the forward-biased junction is limited by introducing a reverse biased potential barrier connected in series with it in a single structure [6]. As a result, the number of carriers injected through the forward-biased junction is equal to the number of photo-generated carriers. In this case, the photosensitivity increases to $S = 10 \text{ A/W}$ with increasing operating voltage U (Fig. 6).

Thus, the basic difference between modified two- and three-barrier structures from classical structures is that their photocurrent appears in the entire voltage range, beginning with the very initial region. In the widely used avalanche photodiodes (AFDs), photocurrent is generated only in the prebreakdown region in a narrow voltage range (near 36 V) (Fig. 7) and their

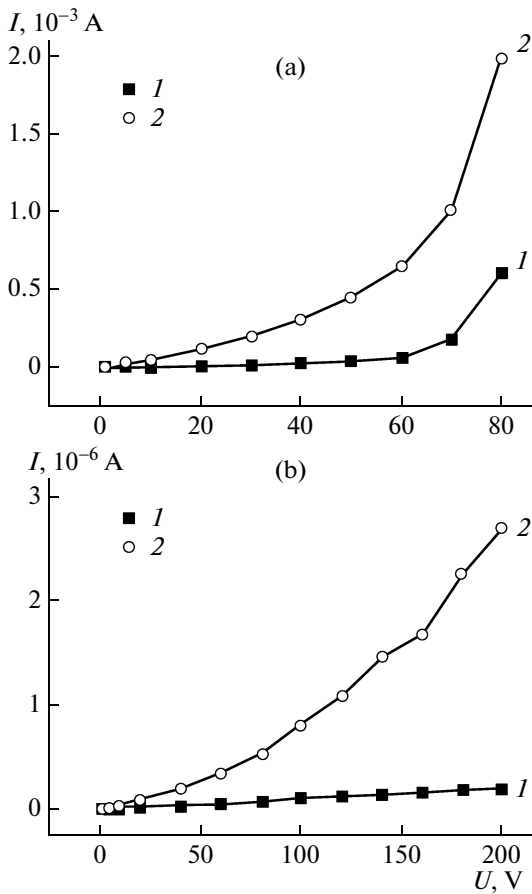


Fig. 5. Current-voltage characteristics of the (a) $p\text{-Al}_{0.08}\text{Ga}_{0.82}\text{As}-n\text{-GaAs-(Au)}$ and (b) (Au)-*n*-AlGaAs-*p*-GaAs-(Ag) structures, measured (1) in the dark and (2) upon exposure of the heterolayer side.

characteristic feature is the operating point drift due to a temperature change with increasing the current density and insignificant fluctuations of the operating voltage [11].

3. EXPERIMENTAL RESULTS AND DISCUSSION

In fact, the multibarrier photodiode is an “amplifier-converter” of weak optical signals to electrical signals. The behavior of the current increase with voltage characterizes the dynamic conductivity steepness, i.e., the ratio of the current increment to the voltage increment,

$$\zeta = \frac{dI}{dU} = d\sigma. \quad (1)$$

Its value is proportional to the multibarrier photodiode photosensitivity, varies according to the dynamic output resistance with operating voltage, and increases with the exposure intensity. The ratio of the

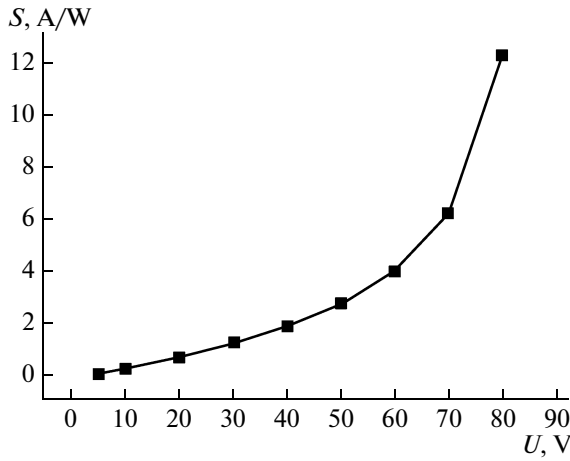


Fig. 6. Dependence of the current photosensitivity S on the voltage U for the (Au + Zn)-p-AlGaAs-n-GaAs-(Sn) heterostructure at a light flux power of 1.62×10^{-4} W.

light and dark steepnesses characterizes the internal photoelectric gain,

$$M = \frac{\zeta_{\text{light}}}{\zeta_{\text{dark}}} \quad (2)$$

The feature of the internal photoelectric amplification effect is that the internal photoelectric gain in multi-barrier photodiodes, depending on the connection mode (current or voltage generator), provides both current and voltage amplification due to the high output resistance of these devices.

In the voltage generator mode, when the load resistance $R_l \rightarrow 0$, for fixed voltages and a proper illuminance, we will observe a photocurrent such as a dark-to-light current step; in this case, the light and dark steepnesses of the dynamic current conductivity are given by

$$\zeta_I^{\text{light}} = \frac{\partial I^{\text{light}}}{\partial U}, \quad (3)$$

$$\zeta_I^{\text{dark}} = \frac{\partial I^{\text{dark}}}{\partial U}, \quad (4)$$

respectively. Substituting expressions (3) and (4) into formula (2), we obtain the internal photocurrent gain,

$$M_I = \frac{\partial I^{\text{light}}}{\partial I^{\text{dark}}} = \frac{I^{\text{light}}_{\max} - I^{\text{light}}_{\min}}{I^{\text{dark}}_{\max} - I^{\text{dark}}_{\min}}. \quad (5)$$

At the same time, since the light current is the sum of the photocurrent and dark current,

$$I^{\text{light}} = I^{\text{photo}} + I^{\text{dark}}, \quad (6)$$

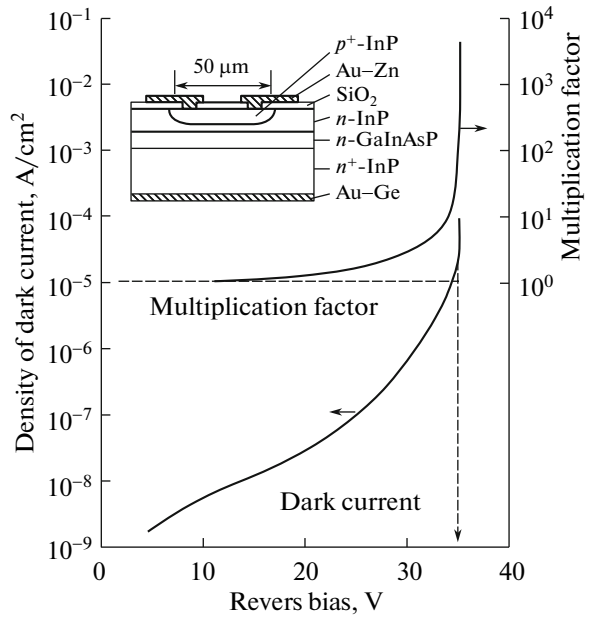


Fig. 7. Dependences of the multiplication factor and dark current density on the reverse bias for the avalanche photodiode with a GaInAsP-based heterostructure.

formula (5) takes the form

$$M_I = \frac{\partial(I^{\text{photo}} + I^{\text{dark}})}{\partial I^{\text{dark}}}. \quad (7)$$

Hence, expressing the photocurrent in terms of the photosensitivity, i.e., the ratio of the photocurrent to the incident light power Φ ,

$$S_I^{\text{photo}} = \frac{I^{\text{photo}}}{\Phi}, \quad (8)$$

we obtain the relation of the photocurrent gain to the photosensitivity

$$M_I = \frac{\partial(I^{\text{photo}} + I^{\text{dark}})}{\partial I^{\text{dark}}} = \frac{\partial(S_I^{\text{photo}} \Phi + I^{\text{dark}})|_{U_2 - U_1}}{(\partial I^{\text{dark}})|_{U_2 - U_1}}. \quad (9)$$

Formula (5) shows that, the lower the dark current increment, the higher the photoelectric gain.

In the current generator mode ($I = \text{const}$), in which case $R_l \rightarrow \infty$, when the photodiode is exposed to light, we obtain a decrease in the load voltage, caused by the difference between dark and light voltages at a given current; hence, we obtain the light and dark steepness of the dynamic voltage conductivity,

$$\zeta_U^{\text{light}} = \frac{\partial I}{\partial U^{\text{light}}}, \quad (10)$$

$$\zeta_U^{\text{dark}} = \frac{\partial I}{\partial U^{\text{dark}}}, \quad (11)$$

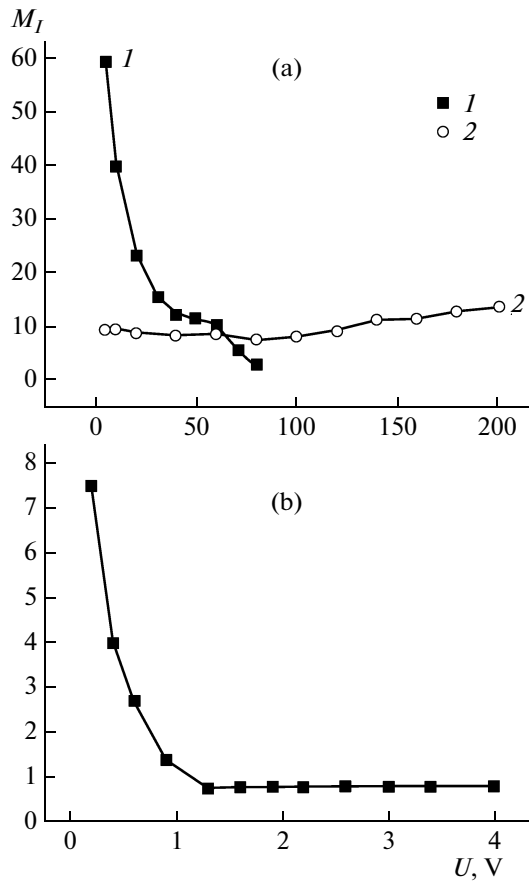


Fig. 8. Dependences of the internal photocurrent gain M_I on the voltage U for (a) two- (1) and three-barrier (2) structures and (b) (Au + Zn)-p-AlGaAs-n-GaAs-(Sn) heterostructure.

respectively. In the case at hand, we obtain the internal photovoltage amplification. Substituting expressions (10) and (11) into formula (2), we obtain the internal photovoltage gain,

$$M_U = \frac{\partial U^{\text{dark}}}{\partial U^{\text{light}}} = \frac{U_{\max}^{\text{dark}} - U_{\min}^{\text{dark}}}{U_{\max}^{\text{light}} - U_{\min}^{\text{light}}}. \quad (12)$$

Systematic features of variations in dark and light currents with voltage in the photodiode structures under study can be accounted for by physical processes in their corresponding regions. For example, in the two-barrier structure, photocarrier generation occurs from the heterolayer, which results in an increase in the charge density in the base region; in the three-barrier structure, photocarriers are generated in the space charge region of the blocking barrier. To explain this effect, we substitute the results obtained from the $I-V$ characteristic data to formulas (5) and (12) and calculate the internal photocurrent and photovoltage gains.

Figure 8a shows that the internal photocurrent gain in the two- and three-barrier structures decreases and

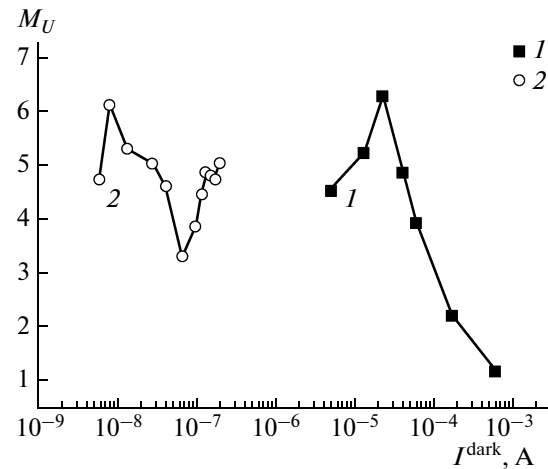


Fig. 9. Dependences of the internal photovoltage gain M_U on the dark current I^{dark} (in the current generator mode) for (1) two- and (2) three-barrier structures.

increases with voltage, respectively. In the single-barrier structure (Fig. 8b), photocurrent amplification takes place in the initial portion of the $I-V$ characteristic; beginning with 1.0 V, amplification is absent due to an increase in the dark current. The observed behavior of internal photoelectric gains is explained by the fact that the dark current component in the two-barrier structure increases with voltage due to carriers arriving at the base region from the heterolayer and due to dark current components of the metal-semiconductor $n-m$ junction (Fig. 5a).

In the three-barrier structure, the thickness of the space charge layer under the metal barrier increases with voltage; the number of photogenerated carriers also proportionally increases (Fig. 5b).

As for the internal photovoltage gain, its increase in the initial portion and its further decrease associated with the behavior of the light (dark) characteristic are inherent to both structures (Fig. 9).

Thus, the internal photoelectric amplification effect is characterized by the current and voltage gains; the former controls the photosensitivity, and the latter follows from the photodiode inclination to amplification of optical signals at a background level.

4. CONCLUSIONS

Thus, in contrast to single-barrier photodiode structures, multibarrier ones exhibit the effect of increasing the number of photogenerated carriers in the entire range of operating voltages, whereas the photocurrent generation in avalanche and injection photodiodes is characterized by the threshold behavior and is associated with changes in the dark-carrier concentration. This interpretation of the internal photoelectric amplification effect will make it possible to estimate experimental current or voltage gains and to

detect internal photoelectric amplification in photodiode structures irrespective of their type.

REFERENCES

1. I. Kim, Opt. Eng. **37**, 3143 (1998).
2. E. M. Dianov et al., Opt. Lett. **15**, 314 (1990).
3. L. V. Asryan and R. S. Suris, Fiz. Tekh. Poluprovodn. **38**, 3 (2004) [Semiconductors **38**, 1 (2004)].
4. A. V. Karimov, D. M. Yodgorova, and E. N. Yakubov, Semicond. Phys. Quant. Electron. Optoelectron. **4**, 378 (2004).
5. C. C. Hodge et al., Semicond. Sci. Technol. **5**, 319 (1990).
6. M. D. Petroff and M. G. Stapelbroek, "Blocked Impurity Band Detectors," US Patent No. 4,568,960; filed Oct. 1980; granted 4 Feb. 1986.
7. A. V. Karimov and D. M. Yodgorova, Radioelectron. Commun. Syst. **2**, 55 (2006).
8. A. V. Karimov and D. A. Karimova, in *Proc. of the Conf. on Materials Science in Semiconductor Processing, Feb.–June, 2003*, vol. 6, Nos. 1–3, p. 137.
9. A. V. Karimov and D. M. Édgorova, Élektronika **11**, 5 (2005).
10. A. V. Karimov, D. M. Édgorova, F. A. Giyasova, T. M. Azimov, U. M. Buzrukov, and A. A. Yakubov, Tekhnol. Konstr. Élektron. Appar. **4**, 23 (2007).
11. K. Nishida, K. Taduchi, and Y. Matsumova, Appl. Phys. Lett. **35**, 251 (1979).

Translated by A. Kazantsev